



Multi-Physics Constraints at Different Densities to Probe Nuclear Symmetry Energy in Hyperonic Neutron Stars

Suprovo Ghosh¹, Bikram Keshari Pradhan¹, Debarati Chatterjee¹ and Jürgen Schaffner-Bielich^{2*}

¹Inter-University Centre for Astronomy and Astrophysics, Pune University Campus, Pune, India, ²Institut für Theoretische Physik, Goethe Universität, Frankfurt, Germany

OPEN ACCESS

Edited by:

Helena Pais,
University of Coimbra, Portugal

Reviewed by:

Isaac Vidana,
Universities and Research, Italy
Adriana Rodica Raduta,
Horia Hulubei National Institute for
Research and Development in Physics
and Nuclear Engineering (IFIN-HH),
Romania

*Correspondence:

Jürgen Schaffner-Bielich
schaffner@astro.uni-frankfurt.de

Specialty section:

This article was submitted to
Nuclear Physics,
a section of the journal
Frontiers in Astronomy and Space
Sciences

Received: 31 January 2022

Accepted: 28 February 2022

Published: 28 March 2022

Citation:

Ghosh S, Pradhan BK, Chatterjee D
and Schaffner-Bielich J (2022) Multi-
Physics Constraints at Different
Densities to Probe Nuclear Symmetry
Energy in Hyperonic Neutron Stars.
Front. Astron. Space Sci. 9:864294.
doi: 10.3389/fspas.2022.864294

The appearance of strangeness in the form of hyperons within the inner core of neutron stars is expected to affect its detectable properties, such as its global structure or gravitational wave emission. This work explores the parameter space of hyperonic stars within the framework of the Relativistic Mean Field model allowed by the present uncertainties in the state-of-the-art nuclear and hypernuclear experimental data. We impose multi-physics constraints at different density regimes to restrict the parameter space: Chiral effective field theory, heavy-ion collision data, and multi-messenger astrophysical observations of neutron stars. We investigate possible correlations between empirical nuclear and hypernuclear parameters, particularly the symmetry energy and its slope, with observable properties of neutron stars. We do not find a correlation for the hyperon parameters and the astrophysical data. However, the inclusion of hyperons generates a tension between the astrophysical and heavy-ion data constraining considerably the available parameter space.

Keywords: symmetry energy, hyperons, neutron stars, equation of state, nuclear, hypernuclear, heavy-ion, multi-messenger

1 INTRODUCTION

Understanding strong interaction among hadrons is one of the most intriguing topics in nuclear physics. Despite the recent progress in understanding the phase diagram of Quantum Chromodynamics (QCD), the theory of strong interactions (Baym et al., 2018; David et al., 2020), we are still far from achieving a unified description of nuclear matter under extreme conditions of density and temperature. While terrestrial nuclear experiments probe densities close to nuclear saturation density ($n_0 \sim 0.16 \text{ fm}^{-3}$) (Gandolfi et al., 2015; Lattimer, 2015), heavy-ion collision (HIC) experiments (Le Fèvre et al., 2016; Russotto et al., 2016) provides information about the hot and dense matter at several times n_0 . Recent progress in Lattice QCD (Inoue, 2016; Inoue, 2019; Fabbietti et al., 2021) also provides new constraints on the properties of matter at high temperature and low densities. Neutron stars, on the contrary, are astrophysical laboratories that provide us an opportunity to investigate ultra-high density (up to 10 times n_0) and low-temperature regime of the QCD phase diagram, given the conditions that exist only in its interior (Lattimer and Prakash, 2004; Glendenning, 2012).

Strangeness adds a new dimension to the description of nuclear matter. The presence of strangeness has already been established in heavy-ion collisions (appearance of hyperons and kaons) or in finite nuclear systems (hypernuclei). It is also conjectured that strangeness-containing

matter, in the form of hyperons, kaons, or even deconfined quark matter, can appear at the ultra-high densities that exist in the core of a neutron star (NS). The appearance of strangeness can have a significant impact on NS composition, structure, and observable astrophysical properties, such as its mass, radius, cooling, or gravitational wave (GW) emission (Oertel et al., 2017).

In order to connect the NS internal composition with its global properties, one requires an equation of state (EoS) (Lattimer, 2012; Lattimer, 2015; Baym et al., 2018). The theoretical description of NS matter, therefore, requires the construction of models of hadron–hadron interaction, using non-relativistic (such as Skyrme or Gogny interactions) (Vautherin and Brink, 1972; Stone and Reinhard, 2007; Dutra et al., 2012) or relativistic (Relativistic Mean Field or Dirac-Brueckner-Hartree-Fock methods) (Serot and Walecka, 1992; Serot and Walecka, 1997) techniques. In the case of microscopic models (such as the Brueckner-Hartree-Fock method), the interactions are rigorously calculated from lowest order term to increasing order. Nevertheless, the poor knowledge of three-nucleon forces limits their applicability to reproduce real astrophysical data. Phenomenological models are more successful, with the model parameters usually constrained at densities close to n_0 and low isospin values (neutron-proton ratio), but the uncertainty increases at larger densities and asymmetries. The nuclear symmetry energy (the difference between the binding energies of symmetric nuclear matter and neutron matter) is a key quantity that governs the difference in the behavior of infinite symmetric nuclear matter and neutron star matter.

Neutron stars are particularly interesting, as they can be observed *via* electromagnetic (X-ray, γ -ray, radio waves) and gravitational waves, opening up a new era of multi-messenger astronomy. Electromagnetic multi-wavelength observations of NSs reveal a wealth of details about its global structure (Demorest et al., 2010; Antoniadis et al., 2013). NS masses can be determined to high precision using post-Keplerian effects in NSs in binary (Thorsett and Chakrabarty, 1999). Traditionally radius measurements from thermal emission suffered from large uncertainties (Özel et al., 2010; Guillot et al., 2013; Steiner et al., 2013), but the recently launched NICER (Neutron Star Interior Composition Explorer) (Arzoumanian et al., 2014; Miller et al., 2019a; Riley et al., 2019; Miller et al., 2021; Riley et al., 2021) mission has improved NS estimates by exploiting a novel scheme of modulation profiles of pulses. Finally, with the recent detection of GWs for the first time from NS-NS (GW170817) (Abbott et al., 2017), NS-BH (GW200105 and GW200115) (Abbott et al., 2021), and GW190425 (Abbott et al., 2020) systems by LIGO (Aasi et al., 2015) and Virgo (Acernese et al., 2014), GW astronomy is allowing us to probe the interior of NSs directly. The tidal deformation of NSs in the strong gravitational field of its binary companion measured during the inspiral phase of the merger depends on the EoS and, therefore, reveals information about its radius and interior composition (Abbott et al., 2018; Annala et al., 2018; Most et al., 2018; Abbott et al., 2019).

In the recent past, there have been several attempts to impose constraints on the NS EoS using data from NS multi-messenger astrophysical observations within a statistical Bayesian scheme (Coughlin et al., 2019; Dietrich et al., 2020; O’Boyle et al., 2020;

Biswas, 2021a; Biswas, 2021b; Biswas et al., 2021; Pang et al., 2021). In such a scheme, the low-density EOS constrained by theoretical and experimental nuclear physics is matched with parametrized high-density EOSs satisfying gravitational wave and electromagnetic data (Tews et al., 2018; Tews et al., 2019a; Tews et al., 2019b; Gandolfi et al., 2019; Capano et al., 2020). Usually, the EoSs are based on different parametrization schemes such as piecewise polytropes (Read et al., 2009; Hebeler et al., 2013; Annala et al., 2018; Gamba et al., 2019), spectral representation (Lindblom, 2018; Fasano et al., 2019), speed-of-sound parametrization (Tews et al., 2018; Greif et al., 2019; Landry et al., 2020), or nuclear meta-modeling technique (Güven et al., 2020). Only a few recent works used the RMF model (Traversi et al., 2020) or hybrid (nuclear + piecewise polytope) parametrizations (Biswas et al., 2021) to obtain posterior distributions of empirical parameters. Correlations among empirical nuclear parameters and some chosen NS observables have only recently been explored (Carson et al., 2019; Xie and Li, 2019; Zhang and Li, 2019; Zimmerman et al., 2020). Although several of these works suggested probing the effect of the presence of hyperons, none of them consistently included hyperons within such a scheme. It, therefore, remains to be investigated whether one can restrict the parameter space of uncertainties associated with hyperons (hypernuclear potentials or hyperon couplings) or if they show any physical correlations with measurable properties such as nuclear saturation parameters or NS astrophysical observables.

In recent work (Ghosh et al., 2022), multi-physics constraints were imposed at different density regimes on the nuclear EoS using a “cut-off scheme,” and correlations of nuclear saturation parameters with astrophysical observables were investigated. Motivated by the Bayesian approach, the parameters of the realistic nuclear model were varied within their allowed uncertainties, compatible with the state-of-the-art nuclear experimental data and the parameter space, constrained using a combination of current best-known physical constraints at different density regimes: theoretical (chiral effective field theory) at low densities, multi-messenger (multi-wavelength electromagnetic as well as GW) astrophysical data at high densities, and experimental (nuclear and heavy-ion collision) at intermediate densities (Tsang et al., 2018; Dexheimer et al., 2021) to restrict the parameter space of the nuclear model. Furthermore, nuclear and heavy-ion collision experiments are isospin symmetric (same number of neutrons and protons), so studying NS matter provides information about the unknown nuclear symmetry energy.

This article extends the above investigation to neutron star matter including strangeness, particularly hyperons. Within the framework of the RMF model and allowing for a parameter space spanning current uncertainties in nuclear and hypernuclear physics, we impose multi-physics constraints in different density regimes from terrestrial nuclear/hypernuclear and multi-messenger astrophysical data. This study aims to investigate possible correlations between empirical nuclear and hypernuclear parameters (particularly the symmetry energy and its slope) with NS astrophysical observables.

The structure of the article is as follows: in **Section 2**, we describe the methods used to determine the composition of NS matter including hyperons in the framework of the RMF model. In **Section 3**, we impose constraints at different densities on the hyperonic EoS. In **Section 4**, we discuss the results of this investigation, and in **Section 5** we discuss the implications of these findings.

2 METHODS

As discussed in **Section 1**, we calculate the beta equilibrated, charge-neutral NS EoS within the RMF framework. For our investigation, we consider the standard baryon octet, as well as electrons and muons. The interaction Lagrangian density (\mathcal{L}) considered in this work is given in **Eq. 1** (Weissenborn et al., 2012; Pradhan and Chatterjee, 2021). In this model, the baryon–baryon interaction is mediated by the exchange of scalar (σ), vector (ω), isovector (ρ) mesons, and the strange baryon. In other words, hyperon–hyperon interactions are carried out by additional strange scalar (σ^*) and strange vector (ϕ) mesons:

$$\begin{aligned} \mathcal{L} = & \sum_B \bar{\psi}_B \left(i\gamma^\mu \partial_\mu - m_B + g_{\sigma B} \sigma - g_{\omega B} \gamma_\mu \omega^\mu - g_{\rho B} \gamma_\mu \vec{I}_B \cdot \vec{\rho}^\mu \right) \psi_B \\ & + \frac{1}{2} \left(\partial_\mu \sigma \partial^\mu \sigma - m_\sigma^2 \sigma^2 \right) - U_\sigma + \frac{1}{2} m_\omega^2 \omega_\mu \omega^\mu - \frac{1}{4} \omega_{\mu\nu} \omega^{\mu\nu} \\ & - \frac{1}{4} \left(\vec{\rho}_{\mu\nu} \cdot \vec{\rho}^{\mu\nu} - 2m_\rho^2 \vec{\rho}_\mu \cdot \vec{\rho}^\mu \right) + \Lambda_\omega \left(g_{\rho N}^2 \vec{\rho}_\mu \cdot \vec{\rho}^\mu \right) \left(g_{\omega N}^2 \omega_\mu \omega^\mu \right) \\ & + \sum_Y \bar{\psi}_Y \left(g_{\sigma^* Y} \sigma^* - g_{\phi Y} \gamma_\mu \phi^\mu \right) \psi_Y + \frac{1}{2} m_\phi^2 \phi_\mu \phi^\mu - \frac{1}{4} \phi_{\mu\nu} \phi^{\mu\nu} \\ & + \frac{1}{2} \left(\partial_\mu \sigma^* \partial^\mu \sigma^* - m_{\sigma^*}^2 \sigma^{*2} \right) + \sum_{\ell=\{e^-, \mu^-\}} \bar{\psi}_\ell \left(i\gamma^\mu \partial_\mu - m_\ell \right) \psi_\ell \end{aligned} \quad (1)$$

where

$$U_\sigma = \frac{1}{3} b m_N (g_{\sigma N} \sigma)^3 + \frac{1}{4} c (g_{\sigma N} \sigma)^4$$

In **Eq. 1**, B stands for the baryon octet ($p, n, \Lambda, \Sigma^-, \Sigma^0, \Sigma^+, \Xi^-, \Xi^0$) whereas Y stands for hyperons ($\Lambda, \Sigma^-, \Sigma^0, \Sigma^+, \Xi^-, \Xi^0$). One can solve the equation of motion governing constituent particle fields (Ψ) as well as those of the following mesons (Hornick et al., 2018; Pradhan and Chatterjee, 2021). Replacing the meson fields with their mean values in RMF framework, the energy density (ϵ) corresponding to the Lagrangian given in **Eq. 1** can be expressed as

$$\begin{aligned} \epsilon = & \frac{1}{2} m_\sigma^2 \bar{\sigma}^2 + \frac{1}{2} m_\omega^2 \bar{\omega}^2 + \frac{1}{2} m_\rho^2 \bar{\rho}^2 + \frac{1}{2} m_{\sigma^*}^2 \bar{\sigma}^{*2} + \frac{1}{2} m_\phi^2 \bar{\phi}^2 \\ & + \frac{1}{3} b m_N (g_{\sigma N} \bar{\sigma})^3 + \frac{1}{4} c (g_{\sigma N} \bar{\sigma})^4 + 3 \Lambda_\omega (g_\rho N g_\omega N \bar{\rho} \bar{\omega})^2 \\ & + \sum_B \frac{g_{sB}}{2\pi^2} \int_0^{k_{FB}} \sqrt{k^2 + m_B^{*2}} dk + \sum_\ell \frac{g_{s\ell}}{2\pi^2} \int_0^{k_{F\ell}} \sqrt{k^2 + m_\ell^2} dk \end{aligned} \quad (2)$$

where g_{si} and k_{Fi} represent the spin degeneracy and Fermi momentum of the i th species, respectively. The baryon effective mass (m_B^*) is then defined as

$m_B^* = m_B - g_{\sigma B} \bar{\sigma} - g_{\sigma^* B} \bar{\sigma}^*$. The pressure can be expressed using Gibbs–Duhem relation:

$$p = \sum_{i=B,\ell} \mu_i n_i - \epsilon \quad (3)$$

with n_i being the number density of i th constituent. The chemical potentials for baryon (μ_B) and lepton (μ_ℓ) are given by

$$\begin{aligned} \mu_B &= \sqrt{k_{FB}^2 + m_B^{*2}} + g_{\omega B} \bar{\omega} + g_{\phi B} \bar{\phi} + I_{3B} g_{\rho B} \bar{\rho} \\ \mu_\ell &= \sqrt{k_{F\ell}^2 + m_\ell^2} \end{aligned} \quad (4)$$

2.1 Nucleonic Matter

The isoscalar nucleon-meson coupling parameters ($g_{\sigma N}$, $g_{\omega N}$, b , and c) are determined by fixing the nuclear saturation parameters: nuclear saturation density (n_0), binding energy per nucleon at saturation (E_{sat}), incompressibility (K_{sat}), and the effective nucleon mass (m^*) at saturation. On the other contrary, the isovector couplings $g_{\rho N}$ and Λ_ω are fixed to the symmetry energy (E_{sym}) and slope of symmetry energy (L_{sym}) at saturation (Chen and Piekarewicz, 2014; Hornick et al., 2018; Ghosh et al., 2022). The range of empirical parameters considered in this work are consistent with the state-of-the-art nuclear experimental data (Ghosh et al., 2022) and are summarized in **Table 1**.

2.2 Hyperonic Matter

In the Lagrangian **Eq. 1**, the attractive interaction among hyperons is mediated by the exchange of strange scalar (σ^*) meson, and the repulsive interaction is mediated by the exchange of strange vector (ϕ) meson. However, it has been concluded that models with attractive hyperon–hyperon interaction show incompatibility with observations of the maximum NS mass (Weissenborn et al., 2012). Hence, we set the strange scalar couplings to 0, i.e., $g_{\sigma^* Y} = 0$, and the remaining non-strange hyperon meson coupling constants ($g_{\sigma Y}$) are fitted to the hyperon-nucleon potential (U_Y) at saturation using **Eq. 5** (Weissenborn et al., 2012). Among the nucleon-hyperon potentials, the best-known potential is that of the hyperon Λ , having a value of $U_\Lambda = -30$ MeV (Millener et al., 1988; Schaffner et al., 1992). Although the potential depths for hyperons Σ and Ξ are not known precisely, it has been concluded that the Σ -nucleon potential is repulsive (Mareš et al., 1995; Schaffner-Bielich and Gal, 2000; Friedman and Gal, 2007) whereas U_Ξ is attractive in nature (Fukuda et al., 1998; Khaustov et al., 2000; Schaffner-Bielich and Gal, 2000). Hence, for this investigation, we vary U_Σ in the range of 0 to +30 MeV and U_Ξ from –30 MeV to 0. The vector hyperon couplings ($g_{\omega Y}$, $g_{\phi Y}$) are fixed to their SU(6) values (see **Eq. 6**) (Schaffner et al., 1993; Weissenborn et al., 2012):

$$U_Y(n_0) = -g_{\sigma Y} \bar{\sigma} + g_{\omega Y} \bar{\omega}, \quad (5)$$

$$\begin{aligned} g_{\omega \Lambda} &= g_{\omega \Sigma} = 2g_{\omega \Xi} = \frac{2}{3} g_{\omega N} \\ 2g_{\phi \Lambda} &= 2g_{\phi \Sigma} = g_{\phi \Xi} = \frac{-2\sqrt{2}}{3} g_{\omega N} \end{aligned} \quad (6)$$

Recent lattice QCD calculations by the HALQCD group extracted hyperon potentials at almost physical quark masses and used it to estimate the hyperon potentials in pure neutron

TABLE 1 | Range (minimum and maximum values) of nuclear and hypernuclear parameters at saturation density used in this work. Masses of mesons and the nucleon are fixed as $m_\sigma = 550$ MeV, $m_\omega = 783$ MeV, $m_\rho = 770$ MeV, $m_\phi = 1020$ MeV and $m_N = 939$ MeV.

n_0 (fm $^{-3}$)	E_{sat} (MeV)	K_{sat} (MeV)	E_{sym} (MeV)	L_{sym} (MeV)	m^* (m_N)	U_Λ (MeV)	U_Σ (MeV)	U_Ξ (MeV)	y
0.14	-16.2	200	28	40	0.55	-30	0	-30	0
0.17	-15.8	300	34	70	0.75	-30	30	0	1

matter and the nuclear matter using the Brueckner-Hartree-Fock approximation (Inoue, 2016; Inoue, 2019). They find that the hyperon potentials in nuclear matter are $U_\Lambda = -28$ MeV, $U_\Sigma = +15$ MeV and $U_\Xi = -4$ MeV. From **Figure 4** in Inoue (2019), one can read off the hyperon potentials for Σ^- and Σ^+ , as well as for Ξ^0 and Ξ^- in pure neutron matter. The relevant potentials for neutron star matter are the ones for the Σ^- and the Ξ^- with the potentials of +25 MeV and +6 MeV, respectively. However, these results suggest that the isovector hyperon coupling ($g_{\rho Y}$) differs from its SU(6) quark model values, where the isospin potential for the Ξ would be as large as the one for nucleons, and the one for the Σ is even twice as large. For a typical nucleon isospin potential of about 32 MeV, one arrives at hyperon isospin potentials, which are more than a factor two larger than those from the HALQCD analysis. We, therefore, introduce a scaling parameter y , which ranges from 0 to 1 (0 to SU(6) coupling strength) to span the uncertainty in the hyperon-isovector coupling. In that case, $g_{\rho Y}$ can be expressed as

$$\begin{aligned} g_{\rho\Lambda} &= 0 \\ \frac{g_{\rho\Sigma}}{g_{\rho N}} &= \frac{1}{2} \frac{g_{\rho\Sigma}}{g_{\rho N}} = y, \quad y \in [0, 1] \end{aligned} \quad (7)$$

The effect of the variation in the y -parameter (isovector hyperon coupling) on the particle fractions can be understood from **Figure 1**. For a chosen parameter set from **Table 1**, Ξ^- starts to appear at 2.27, 2.34, and 2.45 n_0 for y values 0, 0.5, and 1, respectively. However, Ξ^0 starts to appear at 6.977, 6.943, and 6.850 n_0 for y changing from 0 to 1 in steps of 0.5. One must note that the threshold of appearance of the hyperons will depend upon the hyperon potentials and the nuclear saturation parameters chosen for the EoS.

2.3 Global Structure

The equilibrium structure of a non-rotating, relativistic NS is obtained by solving the coupled equations of hydrostatic equilibrium known as the Tolman-Oppenheimer-Volkoff (TOV) equations (Glendenning, 2012; Schaffner-Bielich, 2020):

$$\begin{aligned} \frac{dm(r)}{dr} &= 4\pi\varepsilon(r)r^2, \\ \frac{dp(r)}{dr} &= -\frac{[p(r) + \varepsilon(r)][m(r) + 4\pi r^3 p(r)]}{r(r - 2m(r))} \end{aligned} \quad (8)$$

with the given equation of state, which gives a relation between the energy density (ε) and pressure (p). These TOV in **Eq. 8** are integrated from the center of the star to the surface with the boundary conditions of vanishing mass, $m|_{r=0} = 0$, at the center of the star, and a vanishing pressure, $p|_{r=R} = 0$, at the surface.

By varying the central density for a given EoS, we can get a sequence of NSs with different mass and radii, thus giving the M-R curves.

The tidal deformability parameter quantifies the degree of the tidal deformation effects due to the companion in coalescing binary NS systems during the early stages of an inspiral. It is defined as

$$\lambda = -\frac{Q_{ij}}{\varepsilon_{ij}} \quad (9)$$

where Q_{ij} is the induced mass quadrupole moment of the NS and ε_{ij} is the gravitational tidal field of the companion. The tidal deformability λ is related to the dimensionless $l = 2$ tidal Love number k_2 as follows (Flanagan and Hinderer, 2008; Hinderer, 2008):

$$\Lambda = \frac{2}{3} k_2 \left(\frac{R}{M} \right)^5 \quad (10)$$

The tidal Love number (k_2) can be obtained by solving a set of differential equations coupled with the TOV equations (Yagi and Yunes, 2013). The total tidal effect of two neutron stars in an inspiraling binary system is given by the mass-weighted (dimensionless) tidal deformability $\tilde{\Lambda}$ defined as (Hinderer et al., 2010)

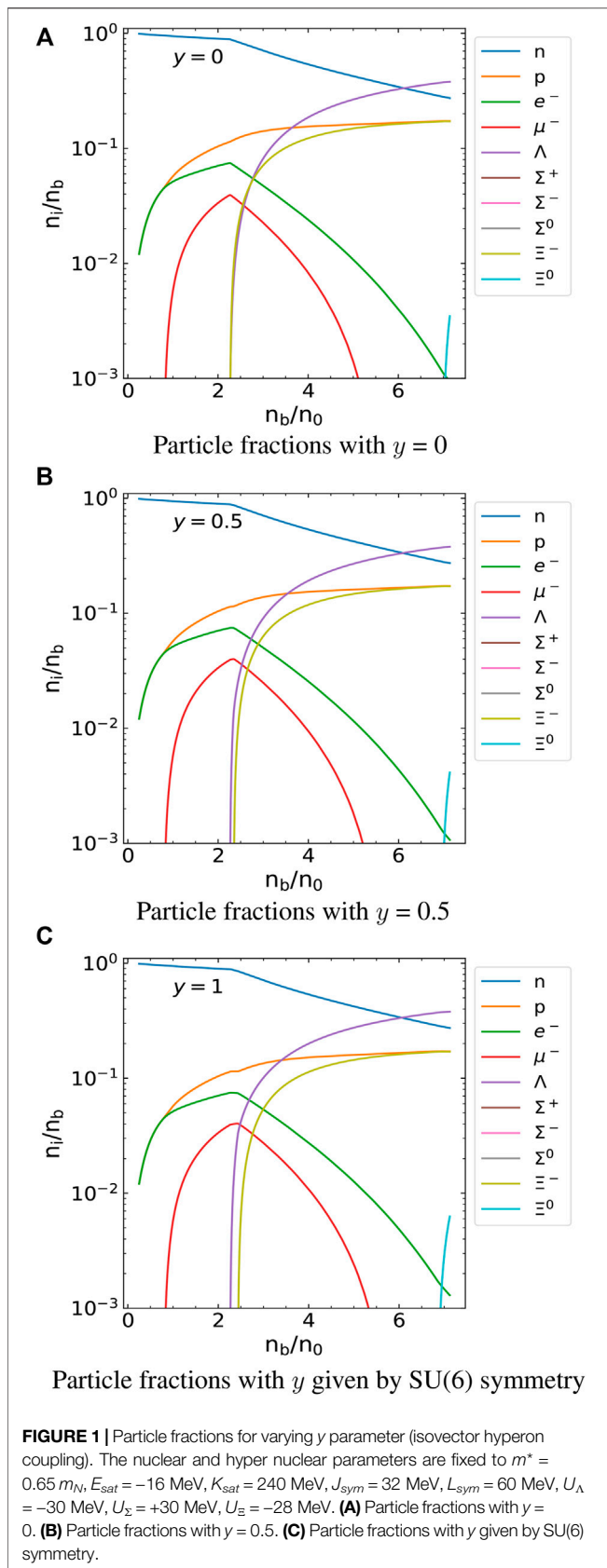
$$\tilde{\Lambda} = \frac{16}{13} \frac{(M_1 + 12M_2)M_1^4\Lambda_1 + (M_2 + 12M_1)M_2^4\Lambda_2}{(M_1 + M_2)^5} \quad (11)$$

where $\Lambda_1 = \Lambda_1(M_1)$ and $\Lambda_2 = \Lambda_2(M_2)$ are the (dimensionless) tidal deformabilities and M_1, M_2 are the masses of the individual binary components, respectively.

3 MULTI-DENSITY CONSTRAINTS

In this work, we constrain the parameter space of the nucleonic and hyperonic matter as described in **Section 2** using a ‘‘cut-off filter’’ scheme where we impose strict limits from nuclear and astrophysical observation to obtain the posteriors. In the language of Bayesian analysis, the priors are obtained by varying the nuclear empirical parameters, hyperon potentials, and isovector couplings uniformly within their uncertainty range in **Table 1**, and the likelihood functions are appropriately chosen physical conditions as the Filter functions described in **Section 3.1**.

Miller et al. (2019b) pointed out the statistical uncertainties in constraining EoS by putting strict limits from multi-messenger observations of neutron stars like we have used here. With many



priors, this cut-off scheme gives a correct estimate of the nuclear parameter ranges consistent with the observations. Recent works (Annala et al., 2018; Most et al., 2018; Annala et al., 2020; Wei et al., 2020; Annala et al., 2021) also used similar cut-off schemes for constraining the EoS of ultra-dense matter. In the recent work by Ghosh et al. (2022), it was explicitly shown that including the statistical re-weighting using χ -squared statistics might change the posterior probability distribution slightly, but it does not significantly alter the physical correlation between nuclear empirical parameters and astrophysical observables. So, we adopt this “cut-off filter” scheme for this work.

3.1 Filter Functions

The following physical constraints at different densities from multi-disciplinary physics are applied in this work:

• At Low Densities: χ EFT

Chiral EFT is an effective theory of QCD that describes strong many-body interactions among nucleons using order by order expansions in terms of contact interactions and long-range pion exchange interactions. In particular, the χ EFT expansion gives estimates of theoretical uncertainties depending on local chiral two and three-nucleon interactions using quantum Monte Carlo methods, which are one of the most precise many-body methods for nuclear physics (Drischler et al., 2016; Drischler et al., 2020). The EoS of pure neutron matter (PNM) can be well constrained at low baryon densities n_b in the range of ~ 0.5 – $1.4 n_0$ (Drischler et al., 2019).

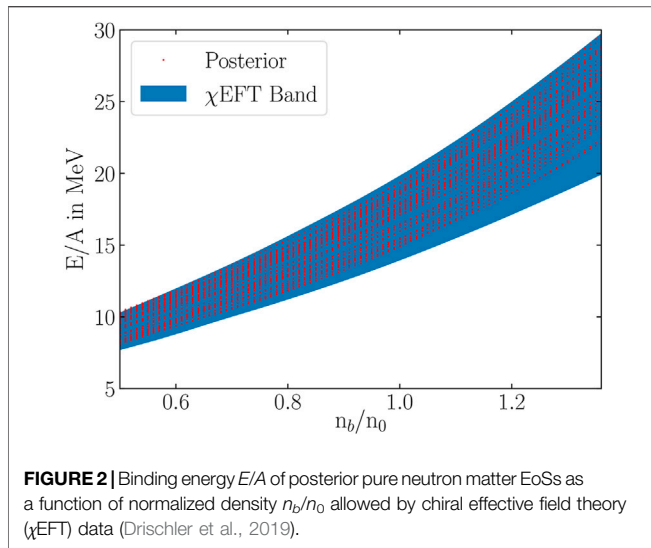
• At High Densities: NS Astrophysical Data

The constraints on the EoS at high density come from multi-messenger astrophysical observations, such as high mass NS observations, GW measurement of tidal deformability from binary neutron star mergers as follows:

- (1) From the recent observations of the heaviest known pulsar PSR J0740+6620, the maximum mass of the neutron stars should be equal to or exceed $2.08_{-0.07}^{+0.07} M_{\odot}$ (Fonseca et al., 2021). This sets an upper bound on the maximum NS masses corresponding to the EoSs considered.
- (2) The recent analyses of the GW170817 event (Abbott et al., 2019) apply a constraint on the upper bound of the effective tidal deformability $\tilde{\Lambda} < 720$ (Tong et al., 2020) using the low-spin highest posterior density interval for tidal deformability. We do not consider the lower limit on tidal deformability in this study. As explained in Section 2.3, the tidal deformability depends on the mass and radius (see Eq. (10)), and therefore this result also leads to a constraint on the mass-radius relation (Annala et al., 2018; Most et al., 2018).

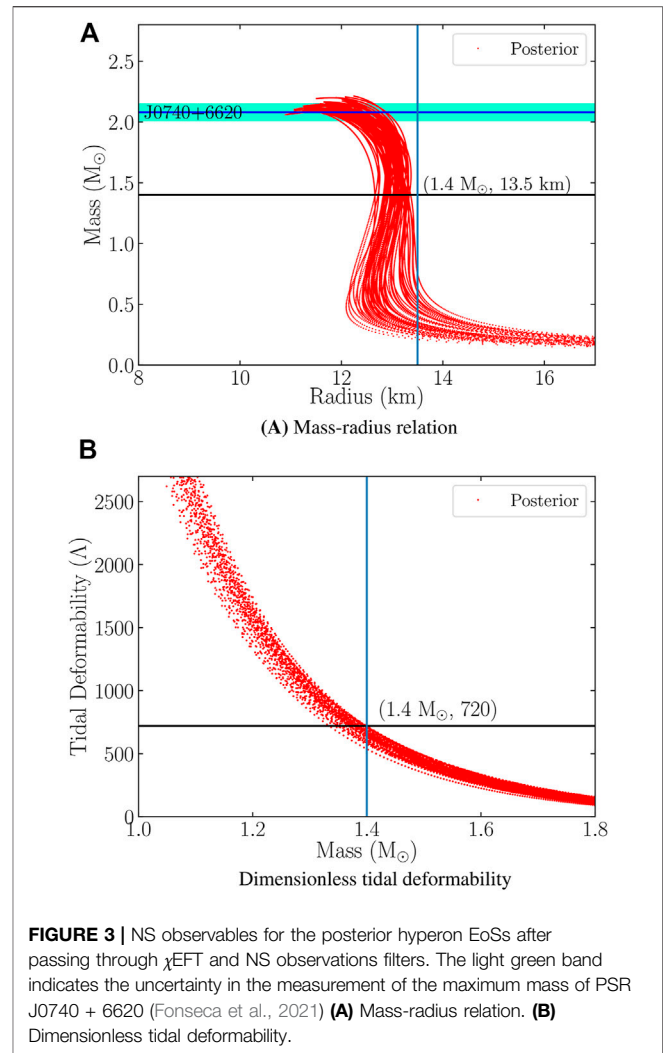
• At Intermediate Densities: Heavy-Ion Collision Experiments

Heavy-ion collision experiments can provide additional information about the behavior of hot dense matter at intermediate densities ~ 1 – $3n_0$. As in our previous



investigation (Ghosh et al., 2022), we impose constraints from three different heavy-ion collision experiments:

- (1) **KaoS experiment:** subthreshold K^+ meson production in Au+Au & C+C nuclear collisions at the Kaon Spectrometer (KaoS) experiment at GSI, Darmstadt (Hartnack et al., 2006) yield kaon multiplicity, which is an indicator of the compressibility of dense matter at densities $\sim 2 - 3n_0$. The analysis of the experimental data using Isospin Quantum Molecular Dynamics (IQMD) transport models points toward a soft EoS (Fuchs et al., 2001; Hartnack et al., 2006) and can be described by a simple Skyrme ansatz with an incompressibility ≤ 200 MeV. The constraint given by the KaoS data implies that only those nucleon potentials, which are more attractive than the Skyrme parametrization within the considered density regime, will be allowed.
- (2) **FOPI experiment:** elliptic flow data in Au+Au collisions between 0.4 and 1.5A GeV by the FOPI collaboration (Le Fèvre et al., 2016) provide constraints for the EoS of compressed symmetric nuclear matter (SNM). By analyzing the FOPI data using IQMD transport codes, one can obtain a constraint for the binding energy of SNM in the density region of $n_b/n_0 \sim 1.4 - 2.0$ (Le Fèvre et al., 2016). In order to impose this constraint, the binding energy for SNM is calculated for the input parameters and only permitted if they lie inside the band allowed by the FOPI data in this density range.
- (3) **ASY-EOS experiment:** information about the symmetry energy for ANM at supra-saturation densities can be obtained from directed and elliptic flows of neutrons and light charged particles measured for the reaction $^{197}\text{Au} + ^{197}\text{Au}$ at 400 MeV/nucleon incident energy within the ASY-EOS experimental campaign at the GSI, Germany (Russotto et al., 2016). In order to impose the ASY-EOS filter, the symmetry energy of ANM EoS is calculated for the input parameters and allowed only if the symmetry energy lies



inside the band allowed by the data in the range of $\sim 1.1 - 2.0n_0$.

3.2 Correlations

Using the posterior obtained from the analysis, we look for any physical correlation of the nuclear parameters, hyperon potentials, and isovector coupling among themselves and also with the astrophysical observables such as the mass and radius of the canonical $1.4M_\odot$ and the massive $2M_\odot$ NS. For this study, we use Pearson's linear correlation coefficient defined as (Kirch, 2008)

$$R_{XY} = \frac{\text{Cov}(X, Y)}{\sqrt{\text{Cov}(X, X)}\sqrt{\text{Cov}(Y, Y)}} \quad (12)$$

where $\text{Cov}(X, Y)$ is the co-variance between two variables X and Y defined as

$$\text{Cov}(X, Y) = \frac{1}{N} \sum_i (X_i - M(X))(Y_i - M(Y)) \quad (13)$$

where N is the number of sample points and $M(X)$ is the mean of the variable X defined as $M(X) = \frac{1}{N} \sum_i X_i$.

4 RESULTS

4.1 Effect of χ EFT + Astro Filters

By randomly varying the parameter space of the nuclear parameters and hyperon potentials from **Table 1**, we generate the uniformly distributed prior set. After generating the random EoSs, we use the χ EFT and astrophysical filters described in **Section 3.1** to obtain filtered sets for the parameters and NS observables. For χ EFT, we evaluate the binding energies in the density range of $n_b/n_0 \sim 0.5$ – 1.4 corresponding to the χ EFT data and allow only those parameter sets that lie within the band allowed by χ EFT calculations (**Figure 2**).

After obtaining the posterior χ EFT, we use the same parameter set to obtain the hyperonic EoS using hyperon potentials and couplings given in **Section 2.2**. We then solve the coupled TOV **Equations 8** and **10** to obtain the mass, radius, and tidal deformability of the NSs. Using the multi-messenger astrophysical and GW observation of NSs given in **Section 3.1**, we rule out further combinations of parameter sets and allow only the combinations that simultaneously satisfy all constraints on NS observables. In **Figure 3**, we plot the mass-radius relations and the dimensionless tidal deformability as a function of NS mass corresponding to the filtered hyperonic EoSs. We can see that NS radii span a wide range from 11 to 14 km.

4.2 Correlations

After obtaining the posterior parameter space, we look for any physical correlation among the parameters and the NS observables as well as within themselves. In **Figure 4**, we display the correlation matrix of the following quantities: nuclear empirical parameters (n_0 , E_{sat} , K_{sat} , E_{sym} , L_{sym}), the effective mass m^*/m , hyperon potentials (U_Σ , U_Ξ), hyperon-isovector coupling parameter γ , and the NS observables ($R_{1.4M_\odot}$, $\Lambda_{1.4M_\odot}$, R_{2M_\odot} , Λ_{2M_\odot}) after applying both χ EFT and astrophysical observations filter. Some of the main observations from the correlation matrix are listed below:

- n_0 and m^*/m show a high correlation (0.71).
- n_0 has a moderate correlation with the NS observables. The correlation is noticeable (0.54) for the constraints for $1.4M_\odot$ NS but is negligible for the constraints for $2M_\odot$.
- Symmetry energy E_{sym} and its slope L_{sym} display a strong correlation (0.79) which only appears when we apply the χ EFT filter. This correlation only comes from the χ EFT filter around saturation density, which is in agreement with previous literature (Hornick et al., 2018; Ghosh et al., 2022).
- We see a moderate correlation (0.44) between L_{sym} and effective mass m^*/m after applying the χ EFT filter.
- The correlation of m^*/m with the NS observables is pretty low (~ 0.1 for $1.4M_\odot$ and ~ 0.3 for $2.0M_\odot$ stars) which is quite the opposite to the purely nucleonic case (Ghosh et al., 2022).
- The correlation between slope of symmetry energy L_{sym} and radius of $1.4M_\odot$ NS is also lower (around 0.4). A correlation between L_{sym} and $R_{1.4M_\odot}$ has been reported in several articles in the literature (Fattoyev et al., 2013; Alam et al., 2016; Lim

and Holt, 2018; Zhu et al., 2018), although recent articles find $R_{1.4M_\odot}$ to be nearly independent of L_{sym} (Hornick et al., 2018; Ghosh et al., 2022).

- All the NS observables (radius and dimensionless tidal deformability for $1.4M_\odot$ and $2M_\odot$ NS), as expected, show a strong correlation with each other (according to **Eq. 9**), although we find a moderate correlation with the observables between $1.4M_\odot$ and $2M_\odot$ NSs.
- We did not find any correlation between the hyperon potentials and the isovector coupling parameter γ with other nuclear parameters and the astrophysical observables.

To understand the correlations better, in **Figure 5**, we plot the posterior distribution of the nuclear parameters (n_0 , E_{sym} , L_{sym} , and m^*/m), which show significant correlations and the astrophysical observables ($R_{1.4M_\odot}$, R_{2M_\odot} , and Λ_{2M_\odot}) after applying both the χ EFT and the astrophysical constraints.

From the corner plots, we see that after applying the χ EFT filter, both the median values of symmetry energy and its slope L_{sym} shift toward a higher value compared to their prior range in **Table 1**, which leads to their strong correlation. For the effective mass, we see that the peak is around 0.63, which is lower than what we observed for purely nucleonic matter (Hornick et al., 2018; Ghosh et al., 2022) because when we include hyperon, the EoSs become softer (Pradhan and Chatterjee, 2021). Therefore, in order to satisfy the astrophysical constraint of maximum mass above $2M_\odot$ and tidal deformability, the posterior of m^*/m shifts toward a lower value. Also, from **Figure 5** in Ghosh et al. (2022), we know that the χ EFT filter removes parameter sets with low effective mass and slope of symmetry energy, which gives rise to a moderate correlation between L_{sym} and m^*/m observed here. For this reason, for the hyperonic case along with the χ EFT filter, the range of effective mass becomes narrow and peaks toward a lower value (around 0.63), which indeed restricts the radius of $1.4M_\odot$ star to 12.6–13.4 km. That is why we observe a very low correlation between m^*/m and the astrophysical observables. We also conclude that there is no correlation between the hyperon potentials (U_Σ , U_Ξ) and the NS astrophysical observables.

4.3 Effect of all Filters: χ EFT + Astro + HIC (KaoS + FOPI + ASY-EOS)

We first generated 50,000 prior sets, and applying all filters (χ EFT, astrophysical data, HIC) obtained almost no posterior sets. In order to understand the effect of the HIC filters, we then passed the prior sets only through the KaoS, FOPI, and ASY-EOS filters and plotted the posterior of each nuclear parameter (see **Figure 6**). From the figures, we observe that, in the K_{sat} distribution, the values are restricted below 240 MeV after HIC filters, which is the effect of the KaoS filter. In the L_{sym} distribution, the values are restricted to > 55 MeV after HIC filters, resulting in a decreased correlation between L_{sym} and E_{sym} . Both these effects were observed in the nucleonic case also and discussed in our previous paper (Ghosh et al., 2022). The most interesting is the distribution of m^*/m . In **Section 4.2**, we noted that including hyperons shifts m^*/m to lower value for astrophysical filters. When we apply HIC filters, we see m^*/m

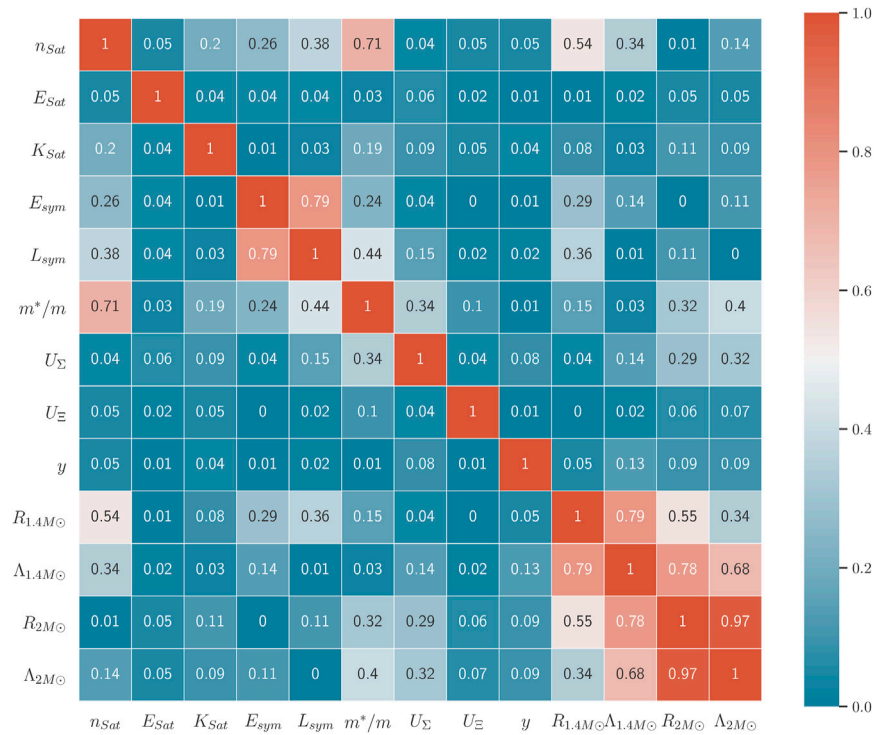


FIGURE 4 | Posterior correlation matrix for variation of nuclear empirical parameters and NS observables, after application of the χ EFT and NS observations filter.

values peak at a higher value around 0.70. The distributions intersect at the two tail ends of the Gaussian curves, giving a very narrow range with low probabilities. This explains why there are so few posterior points due to the combined filters.

In order to obtain a correlation plot after applying all filters, we generated a very large number (2 million) of priors after restricting the prior range to m^*/m to 0.64–0.7 and managed to obtain 200 posterior sets. The resulting correlation plot with this set is given in **Figure 7**. We see that the effects of the HIC filters on correlations are the same as in the nucleonic case (Ghosh et al., 2022): decrease in $L_{sym} - E_{sym}$ correlation, increase in n_0 correlation with NS astrophysical observables, and increase in $K_{sat} - m^*/m$ correlation. We checked that allowing for hyperons means that hyperons appear in all the cases investigated; Λ hyperons always appear close to $2n_0$, while the threshold for the appearance of Σ and Ξ hyperons depends on the value of the corresponding hyperon potentials. One may also note that, for $1.4M_{\odot}$ stars, the fraction of hyperons in the core is lower than in more massive $2M_{\odot}$ stars.

5 DISCUSSION

5.1 Summary of Present Results

The motivation of this study is to investigate any existing correlations between empirical nuclear and hypernuclear parameters (particularly the symmetry energy and its slope) and with NS multi-messenger astrophysical observables such as its mass, radius, and tidal deformability. To this aim, we

extended our previous investigation (Ghosh et al., 2022) from nucleonic to hyperonic matter in NSs. In other words, within the framework of the RMF model, we constrained the parameter space allowed by current uncertainties in nuclear and hypernuclear physics by imposing multi-physics constraints at different density regimes: chiral effective field theory at low densities, astrophysical constraints at high densities, and heavy-ion collision data at intermediate energies.

First, using the filtered EoSs satisfying constraints from both χ EFT and astrophysical data, we searched for any physical correlation among the parameters and the NS observables, as well as among themselves. We found that the effective nucleon mass m^*/m and saturation nuclear density n_0 show a strong correlation. We found n_0 to be moderately correlated with radius and tidal deformability of $1.4M_{\odot}$ NSs, but weakly correlated with those of $2M_{\odot}$ stars. The correlation of m^*/m with the NS observables was low, contrary to the purely nucleonic case. Interestingly, the symmetry energy E_{sym} and its slope L_{sym} showed a significant correlation after imposing the χ EFT filter. There is a non-negligible correlation of m^*/m with L_{sym} .

On applying all filters from χ EFT, astrophysical and heavy-ion data, we found that very few nuclear parameter sets can satisfy all constraints simultaneously. By monitoring the individual posterior distributions of the nuclear saturation parameters, we confirmed the existence of a “tension” between the constraints from the first two filters with those of heavy-ion data. The values of K_{sat} are restricted to below 240 MeV due to the KaoS constraint and L_{sym} to values larger than 55 MeV, drastically reducing the

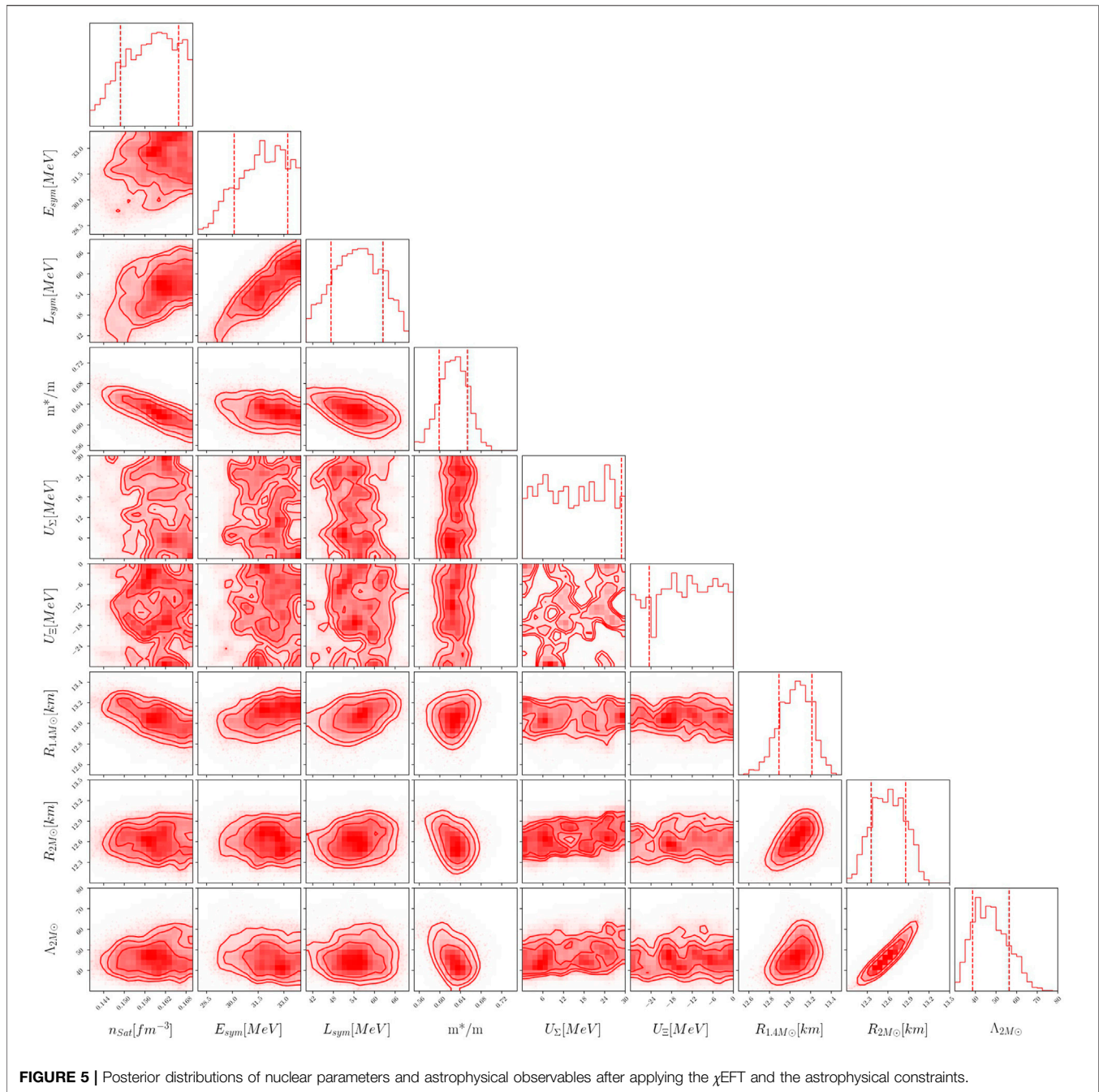


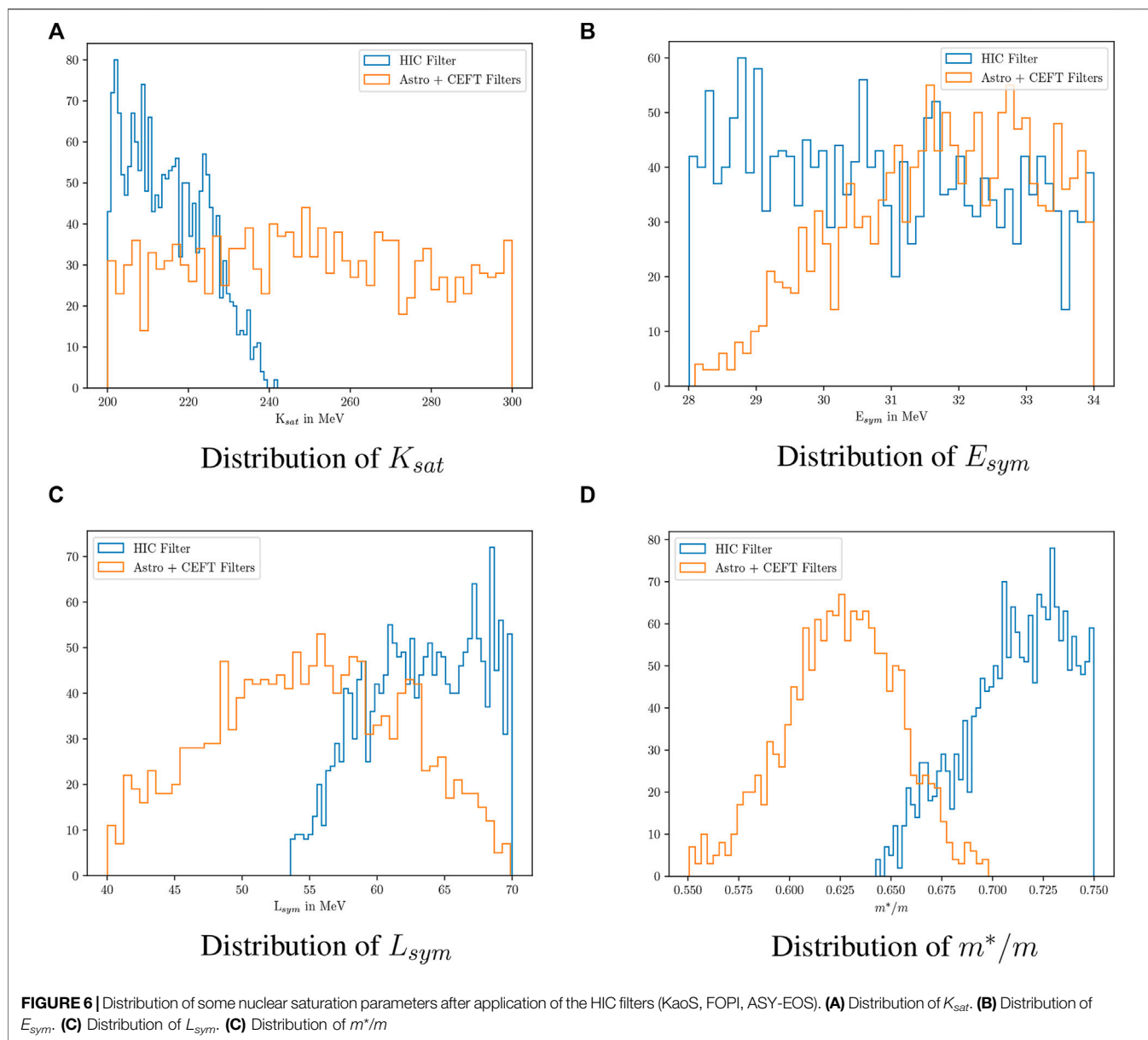
FIGURE 5 | Posterior distributions of nuclear parameters and astrophysical observables after applying the χ EFT and the astrophysical constraints.

available parameter space. Further, low values of m^*/m are allowed by astrophysical filters, while heavy-ion data allow large values. The overall effect of applying the heavy-ion filters was the same as in the nucleonic case (Ghosh et al., 2022): a decreased $L_{sym} - E_{sym}$ correlation, increased n_0 correlation with NS astrophysical observables, and enhanced $K_{sat} - m^*/m$ correlation.

5.2 Comparison With Prior Research

There are several contrasting results in the hyperonic case compared with the nucleonic case (Ghosh et al., 2022).

Mainly, we found a decreased correlation of m^*/m with the NS observables and an increased correlation of n_0 with m^*/m and NS observables for $1.4M_\odot$ NS. Radii and dimensionless tidal deformability (for $1.4M_\odot$ and $2M_\odot$) show a strong correlation with each other, as expected. However, we find a moderate correlation with observables of $1.4M_\odot$ with $2M_\odot$ stars because of the reduced range of radii for hyperonic stars. We checked that the distribution of m^*/m shifts to lower values (peak around 0.63) in posteriors for hyperons compared to nucleons, which peak around 0.7, restricting values of $R_{1.4M_\odot}$ to a reduced range ≈ 13 km. The correlation between the slope of symmetry energy



L_{sym} and radius of $1.4M_{\odot}$ NS is also lower than that in the nucleonic case. A correlation between L_{sym} and $R_{1.4M_{\odot}}$ was reported in several articles in the literature (Fattoyev et al., 2013; Alam et al., 2016; Lim and Holt, 2018; Zhu et al., 2018), although recent articles find $R_{1.4M_{\odot}}$ to be nearly independent of L_{sym} (Hornick et al., 2018; Ghosh et al., 2022). Finally, the astrophysical observables studied in this work (mass, radius, tidal deformability) do not seem to provide correlations with hyperon potentials or the isovector coupling parameter γ . However, one must note that this is not generic for all astrophysical observables. One has to look for other observables, which are sensitive to the hyperon content in the NS interior, such as r -modes, cooling, and thermal evolution (Chatterjee and Vidaña, 2016).

In another recent work (Traversi et al., 2020), Bayesian inference of the NS EoS was performed within the RMF model using astrophysical and nuclear saturation data. Using a selected class of nucleonic models with five empirical parameters and exploring different types of priors, they reported that the EoSs with the largest evidence were the ones featuring a strong reduction of the nucleon effective mass. However, the major drawback of this model was the omission of interaction terms (Λ_{ω} in our work) in the Lagrangian, due to which other saturation parameters, such as symmetry energy or its slope, were not included. A preliminary investigation of the effect of hyperons was also performed by switching on only the Λ hyperon, with a fixed potential depth and coupling constants. However, the effect of the other baryons of the octet and variation of the couplings

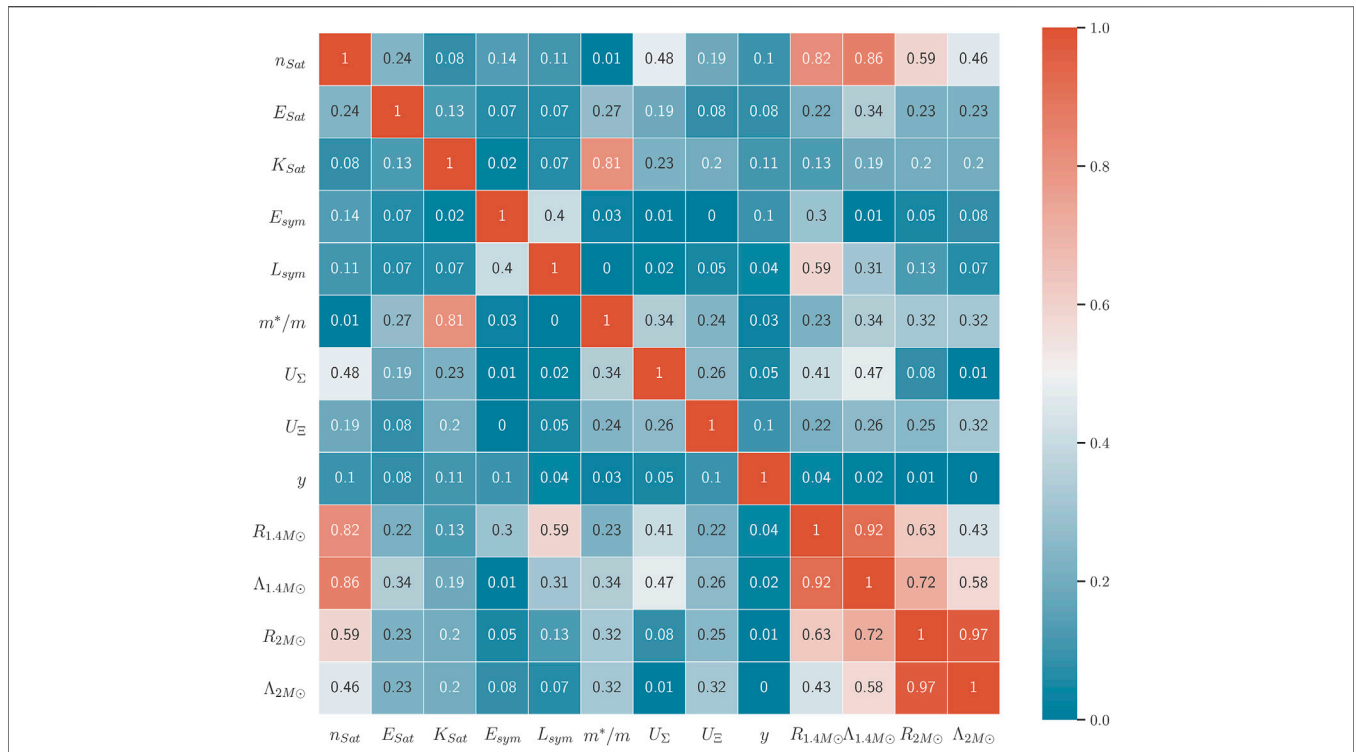


FIGURE 7 | Posterior correlation matrix for variation of nuclear empirical parameters and NS observables, after application of the χ EFT, HIC, and NS observations filters.

and their correlations with other nuclear saturation parameters or NS observables were unexplored.

Another recent study (Güven et al., 2020) used Bayesian statistics to combine low-density nuclear physics data, such as the *ab initio* χ EFT predictions and the isoscalar giant monopole resonance, with astrophysical NS data, within the “meta-model” approach for the dense matter EoS. The posterior probability distribution functions were marginalized over several higher-order nuclear empirical parameters (L_{sym} , K_{sym} , Q_{sat} , Q_{sym}) and observational quantities such as a radius of $1.4M_{\odot}$ NS. This study also explored correlations among $L_{sym} - K_{sym}$ and $K_{sat} - Q_{sym}$ parameters and reported marked tension between astrophysical and nuclear physics constraints. Biswas (2021b) combined laboratory experiments and NS astrophysical observation using Bayesian statistics along with the LIGO/Virgo and NICER observations within a hybrid nuclear + piecewise polytrope (PP) EoS parameterization. This work reported a very weak correlation between L_{sym} and $R_{1.4M_{\odot}}$. Recently, Huth et al. (2021) used a Bayesian inference technique to analyze the nuclear EoS and NS properties, combining data from heavy-ion collisions (FOPI (Le Fèvre et al., 2016) and ASY-EOS (Rusotto et al., 2016) experiments, EoS constraint for symmetric nuclear matter (Danielewicz et al., 2002)), microscopic χ EFT calculations, and multi-messenger information from NICER and XMM Newton missions, as well as GW data and the associated kilonova AT2017gfo9.

The study concluded that HIC constraints are in excellent agreement with NICER observations. However, hyperons were not considered in the above investigations.

5.3 Limitations and Future Directions

In this work, the correlations between nuclear and hypernuclear parameters and NS astrophysical observables have been explored within the framework of the Relativistic Mean Field model. Although the advantage of this realistic phenomenological model is that, unlike polytropic or parametrized EoSs, the results provide important understanding of the underlying nuclear physics, it, however, remains to be established whether such physical correlations are also found in other realistic EoS models in order to generalize the results of this investigation. It would be interesting, for example, to see whether the conclusions would still hold for a Lagrangian with density-dependent couplings. Such possibilities will be addressed in a forthcoming publication. We recall here that the constraints from heavy-ion data are model-dependent and should therefore be treated on a different footing from astrophysical constraints and their implications on the results discussed with a word of caution.

In the future, improved measurements of hyperon potentials in hypernuclear experiments, such as GSI in Germany, JLAB in the United States, and J-PARC in Japan (Chatterjee and Vidaña, 2016), will reduce the uncertainties in the hyperon-nucleon and hyperon-hyperon coupling strengths. With the advent of multi-

messenger astronomy, new upcoming observations of NS properties will also help provide more stringent constraints on the dense matter EoS in NSs.

DATA AVAILABILITY STATEMENT

The original contributions presented in the study are included in the article/Supplementary Material, further inquiries can be directed to the corresponding author.

AUTHOR CONTRIBUTIONS

SG and BP contributed equally to this work and shared first authorship. DC and JS-B shared senior authorship and contributed to the conception of the study. DC was the corresponding author of this article. Both SG and BP performed the theoretical, numerical, and statistical analysis. DC wrote the first draft. SG and BP wrote sections of the

manuscript. All authors contributed to manuscript revision and read and approved the submitted version.

FUNDING

This work was supported by the Deutsche Forschungsgemeinschaft (DFG, German Research Foundation) through the CRC-TR 211 “Strong-Interaction Matter Under Extreme Conditions” – project number 315477589—TRR 211.

ACKNOWLEDGMENTS

DC is grateful to the hospitality of the Institut für Theoretische Physik, J. W. Goethe Universität Frankfurt, Germany, where this work was carried out within the collaborative project “Astrophysical Constraints for Hyperons in Neutron Stars.” SG, BP, and DC acknowledge the usage of the IUCAA HPC computing facility for numerical calculations.

REFERENCES

- Aasi, J., Abbott, B. P., Abbott, R., Abbott, T., Abernathy, M. R., Ackley, K., et al. (2015). Advanced LIGO. *Classical Quan. Gravity* 32, 074001. doi:10.1088/0264-9381/32/7/074001
- Abbott, B. P., et al. (2017). Gw170817: Observation of Gravitational Waves from a Binary Neutron star Inspiral. *Phys. Rev. Lett.* 119, 161101. doi:10.1103/PhysRevLett.119.161101
- Abbott, B. P., Abbott, R., Abbott, T. D., Acernese, F., Ackley, K., Adams, C., et al. (2018). Gw170817: Measurements of Neutron star Radii and Equation of State. *Phys. Rev. Lett.* 121, 161101. doi:10.1103/PhysRevLett.121.161101
- Abbott, B., Abbott, R., Abbott, T., Acernese, F., Ackley, K., Adams, C., et al. (2019). Properties of the Binary Neutron star Merger Gw170817. *Phys. Rev. X* 9, 011001. doi:10.1103/PhysRevX.9.011001
- Abbott, B. P., Abbott, R., Abbott, T. D., Abraham, S., Acernese, F., Ackley, K., et al. (2020). GW190425: Observation of a Compact Binary Coalescence with Total Mass $\sim 3.4 M$. *Astrophys. J. Lett.* 892, L3. doi:10.3847/2041-8213/ab75f5
- Abbott, R., Abbott, T. D., Abraham, S., Acernese, F., Ackley, K., Adams, A., et al. (2021). Observation of Gravitational Waves from Two Neutron star–black Hole Coalescences. *Astrophys. J. Lett.* 915, L5. doi:10.3847/2041-8213/ac082e
- Acernese, F., Agathos, M., Agatsuma, K., Aisa, D., Allemandou, N., Allocca, A., et al. (2014). Advanced Virgo: a Second-Generation Interferometric Gravitational Wave Detector. *Classical Quan. Gravity* 32, 024001. doi:10.1088/0264-9381/32/2/024001
- Alam, N., Agrawal, B. K., Fortin, M., Pais, H., Providência, C., Raduta, A. R., et al. (2016). Strong Correlations of Neutron star Radii with the Slopes of Nuclear Matter Incompressibility and Symmetry Energy at Saturation. *Phys. Rev. C* 94, 052801. doi:10.1103/PhysRevC.94.052801
- Annala, E., Gorda, T., Kurkela, A., and Vuorinen, A. (2018). Gravitational-wave Constraints on the neutron-star-matter Equation of State. *Phys. Rev. Lett.* 120, 172703. doi:10.1103/PhysRevLett.120.172703
- Annala, E., Gorda, T., Kurkela, A., Nättilä, J., and Vuorinen, A. (2020). Evidence for Quark-Matter Cores in Massive Neutron Stars. *Nat. Phys.* 16, 907–910. doi:10.1038/s41567-020-0914-9
- Annala, E., Gorda, T., Katerini, E., Kurkela, A., Nättilä, J., Paschalidis, V., et al. (2021). Multimessenger Constraints for Ultra-dense Matter. arXiv e-prints. arXiv:2105.05132.
- Antoniadis, J., Freire, P. C. C., Wex, N., Tauris, T. M., Lynch, R. S., van Kerkwijk, M. H., et al. (2013). A Massive Pulsar in a Compact Relativistic Binary. *Science* 340, 1233232. doi:10.1126/science.1233232
- Arzoumanian, Z., Gendreau, K. C., Baker, C. L., Cazeau, T., Hestnes, P., Kellogg, J. W., et al. (2014). “The Neutron star interior Composition Explorer (NICER): mission Definition,” in *Space Telescopes and Instrumentation 2014: Ultraviolet to Gamma Ray*. Editors T. Takahashi, J. W. A. den Herder, and M. Bautz (Montréal, QC, Canada: SPIE), 9144, 914420. doi:10.1117/12.2056811
- Baym, G., Hatsuda, T., Kojo, T., Powell, P. D., Song, Y., and Takatsuka, T. (2018). From Hadrons to Quarks in Neutron Stars: a Review. *Rep. Prog. Phys.* 81, 056902. doi:10.1088/1361-6633/aaae14
- Biswas, B., Char, P., Nandi, R., and Bose, S. (2021). Towards Mitigation of Apparent Tension between Nuclear Physics and Astrophysical Observations by Improved Modeling of Neutron star Matter. *Phys. Rev. D* 103, 103015. doi:10.1103/physrevd.103.103015
- Biswas, B. (2021). Impact of PREX-II and Combined Radio/NICER/XMM-Newton’s Mass–Radius Measurement of PSR J0740+6620 on the Dense-Matter Equation of State. *Astrophys. J.* 921, 63. doi:10.3847/1538-4357/ac1c72
- Biswas, B. (2021). Bayesian Model-Selection of Neutron star Equation of State Using Multi-Messenger Observations. arXiv e-prints. arXiv:2106.02644.
- Capano, C. D., Tews, I., Brown, S. M., Margalit, B., De, S., Kumar, S., et al. (2020). Stringent Constraints on Neutron-star Radii from Multimessenger Observations and Nuclear Theory. *Nat. Astron.* 4, 625–632. doi:10.1038/s41550-020-1014-6
- Carson, Z., Steiner, A. W., and Yagi, K. (2019). Constraining Nuclear Matter Parameters with Gw170817. *Phys. Rev. D* 99, 043010. doi:10.1103/PhysRevD.99.043010
- Chatterjee, D., and Vidana, I. (2016). Do hyperons Exist in the interior of Neutron Stars? *Eur. Phys. J. A* 52, 29. doi:10.1140/epja/i2016-16029-x
- Chen, W. C., and Piekarewicz, J. (2014). Building Relativistic Mean Field Models for Finite Nuclei and Neutron Stars. *Phys. Rev. C* 90, 044305. doi:10.1103/PhysRevC.90.044305
- Coughlin, M. W., Dietrich, T., Margalit, B., and Metzger, B. D. (2019). Multimessenger Bayesian Inference of a Binary Neutron star Merger. *Monthly Notices R. Astronom. Soc. Lett.* 489, L91–L96. doi:10.1093/mnras/slz133
- Danielewicz, P., Lacey, R., and Lynch, W. G. (2002). Determination of the Equation of State of Dense Matter. *Science* 298, 1592–1596. doi:10.1126/science.1078070
- David, B., Alexander, A., Alexandra, F., and Hovik, G. (2020). *Compact Stars in the QCD Phase Diagram*. Basel, Switzerland: Universe. doi:10.3390/books978-3-03921-959-9
- Demorest, P. B., Pennucci, T., Ransom, S. M., Roberts, M. S. E., and Hessels, J. W. T. (2010). A Two-Solar-Mass Neutron star Measured Using Shapiro Delay. *Nature* 467, 1081–1083. doi:10.1038/nature09466

- Dexheimer, V., Noronha, J., Noronha-Hostler, J., Yunes, N., and Ratti, C. (2021). Future Physics Perspectives on the Equation of State from Heavy Ion Collisions to Neutron Stars. *J. Phys. G: Nucl. Part. Phys.* 48, 073001. doi:10.1088/1361-6471/abe104
- Dietrich, T., Coughlin, M. W., Pang, P. T. H., Bulla, M., Heinzl, J., Issa, L., et al. (2020). Multimessenger Constraints on the Neutron-star Equation of State and the Hubble Constant. *Science* 370, 1450–1453. doi:10.1126/science.abb4317
- Drischler, C., Carbone, A., Hebeler, K., and Schwenk, A. (2016). Neutron Matter from Chiral Two- and Three-Nucleon Calculations up to $N^3\text{LO}$. *Phys. Rev. C* 94, 054307. doi:10.1103/PhysRevC.94.054307
- Drischler, C., Hebeler, K., and Schwenk, A. (2019). Chiral Interactions up to Next-To-Next-To-Next-To-Leading Order and Nuclear Saturation. *Phys. Rev. Lett.* 122, 042501. doi:10.1103/PhysRevLett.122.042501
- Drischler, C., Furnstahl, R. J., Melendez, J. A., and Phillips, D. R. (2020). How Well Do We Know the Neutron-Matter Equation of State at the Densities inside Neutron Stars? a Bayesian Approach with Correlated Uncertainties. *Phys. Rev. Lett.* 125, 202702. doi:10.1103/PhysRevLett.125.202702
- Dutra, M., Lourenço, O., Sá Martins, J. S., Delfino, A., Stone, J. R., and Stevenson, P. D. (2012). Skyrme Interaction and Nuclear Matter Constraints. *Phys. Rev. C* 85, 035201. doi:10.1103/PhysRevC.85.035201
- Fabbietti, L., Sarti, V. M., and Doce, O. V. (2021). Study of the strong Interaction Among Hadrons with Correlations at the LHC. *Ann. Rev. Nucl. Part. Sci.* 71, 377–402. doi:10.1146/annurev-nucl-102419-034438
- Fasano, M., Abdelsalhin, T., Maselli, A., and Ferrari, V. (2019). Constraining the Neutron star Equation of State Using Multiband Independent Measurements of Radii and Tidal Deformabilities. *Phys. Rev. Lett.* 123, 141101. doi:10.1103/physrevlett.123.141101
- Fattoyev, F. J., Carvajal, J., Newton, W. G., and Li, B. A. (2013). Constraining the High-Density Behavior of the Nuclear Symmetry Energy with the Tidal Polarizability of Neutron Stars. *Phys. Rev. C* 87, 015806. doi:10.1103/PhysRevC.87.015806
- Flanagan, E. E., and Hinderer, T. (2008). Constraining Neutron-star Tidal Love Numbers with Gravitational-Wave Detectors. *Phys. Rev. D* 77, 021502. doi:10.1103/PhysRevD.77.021502
- Fonseca, E., Cromartie, H. T., Pennucci, T. T., Ray, P. S., Kirichenko, A. Y., Ransom, S. M., et al. (2021). Refined Mass and Geometric Measurements of the High-Mass PSR J0740+6620. *Astrophys. J. Lett.* 915, L12. doi:10.3847/2041-8213/ac03b8
- Friedman, E., and Gal, A. (2007). In-medium Nuclear Interactions of Low-Energy Hadrons. *Phys. Rep.* 452, 89–153. doi:10.1016/j.physrep.2007.08.002
- Fuchs, C., Faessler, A., Zabrodin, E., and Zheng, Y. M. (2001). Probing the Nuclear Equation of State by K^+ Production in Heavy-Ion Collisions. *Phys. Rev. Lett.* 86, 1974–1977. doi:10.1103/PhysRevLett.86.1974
- Fukuda, T., Higashi, A., Matsuyama, Y., Nagoshi, C., Nakano, J., Sekimoto, M., et al. (1998). Cascade Hypernuclei in the (K^-, K^+) Reaction on ^{12}C . *Phys. Rev. C* 58, 1306–1309. doi:10.1103/physrevc.58.1306
- Gamba, R., Read, J. S., and Wade, L. E. (2019). The Impact of the Crust Equation of State on the Analysis of GW170817. *Classical Quan. Gravity* 37, 025008. doi:10.1088/1361-6382/ab5ba4
- Gandolfi, S., Gezerlis, A., and Carlson, J. (2015). Neutron Matter from Low to High Density. *Annu. Rev. Nucl. Part. Sci.* 65, 303–328. doi:10.1146/annurev-nucl-102014-021957
- Gandolfi, S., Lippuner, J., Steiner, A. W., Tews, I., Du, X., and Al-Mamun, M. (2019). From the Microscopic to the Macroscopic World: from Nucleons to Neutron Stars. *J. Phys. G: Nucl. Part. Phys.* 46, 103001. doi:10.1088/1361-6471/ab29b3
- Ghosh, S., Chatterjee, D., and Schaffner-Bielich, J. (2022). Imposing Multi-Physics Constraints at Different Densities on the Neutron Star Equation of State. *Eur. Phys. J. A* 58, 37.
- Glendenning, N. (2012). *Compact Stars: Nuclear Physics, Particle Physics and General Relativity*. Astronomy and Astrophysics Library. New York: Springer.
- Greif, S. K., Raaijmakers, G., Hebeler, K., Schwenk, A., and Watts, A. L. (2019). Equation of State Sensitivities when Inferring Neutron star and Dense Matter Properties. *Monthly Notices R. Astronom. Soc.* 485, 5363–5376. doi:10.1093/mnras/stz654
- Guillot, S., Servillat, M., Webb, N. A., and Rutledge, R. E. (2013). Measurement of the Radius of Neutron Stars with High Signal-To-Noise Quiescent Low-Mass X-ray Binaries in Globular Clusters. *Astrophys. J.* 772, 7. doi:10.1088/0004-637x/772/1/7
- Güven, H., Bozkurt, K., Khan, E., and Margueron, J. (2020). Multimessenger and Multiphysics Bayesian Inference for the Gw170817 Binary Neutron star Merger. *Phys. Rev. C* 102, 015805. doi:10.1103/PhysRevC.102.015805
- Hartnack, C., Oeschler, H., and Aichelin, J. (2006). Hadronic Matter Is Soft. *Phys. Rev. Lett.* 96, 012302. doi:10.1103/PhysRevLett.96.012302
- Hebeler, K., Lattimer, J. M., Pethick, C. J., and Schwenk, A. (2013). Equation of State and Neutron star Properties Constrained by Nuclear Physics and Observation. *Astrophys. J.* 773, 11. doi:10.1088/0004-637x/773/1/11
- Hinderer, T., Lackey, B. D., Lang, R. N., and Read, J. S. (2010). Tidal Deformability of Neutron Stars with Realistic Equations of State and Their Gravitational Wave Signatures in Binary Inspiral. *Phys. Rev. D* 81, 123016. doi:10.1103/PhysRevD.81.123016
- Hinderer, T. (2008). Tidal Love Numbers of Neutron Stars. *Astrophys. J.* 677, 1216–1220. doi:10.1086/533487
- Hornick, N., Tolos, L., Zacchi, A., Christian, J. E., and Schaffner-Bielich, J. (2018). Relativistic Parameterizations of Neutron Matter and Implications for Neutron Stars. *Phys. Rev. C* 98, 065804. doi:10.1103/PhysRevC.98.065804
- Huth, S., Pang, P. T. H., Tews, I., Dietrich, T., Le Fèvre, A., Schwenk, A., et al. (2021). Constraining Neutron-Star Matter with Microscopic and Macroscopic Collisions. arXiv e-prints. arXiv:2107.06229.
- Inoue, T. (2016). “Hyperon Single-Particle Potentials from QCD on Lattice,” in PoS INPC, 2016, Adelaide, SA, Australia, September 11–16, 2016, 277. doi:10.22323/1.281.0277
- Inoue, T. (2019). Hyperon Forces from QCD and Their Applications. *JPS Conf. Proc.* 26, 023018. doi:10.7566/jpscp.26.023018
- Khaustov, P., Alburger, D. E., Barnes, P. D., Bassalleck, B., Berdoz, A. R., Biglan, A., et al. (2000). Evidence of Ξ Hypernuclear Production in the $12\text{C}(K^-, K^+)12\text{E}$ Be Reaction. *Phys. Rev. C* 61, 054603. doi:10.1103/physrevc.61.027601
- Kirch, W. (2008). *Pearson's Correlation Coefficient*. Dordrecht: Springer Netherlands, 1090–1091. doi:10.1007/978-1-4020-5614-7_2569
- Landry, P., Essick, R., and Chatziioannou, K. (2020). Nonparametric Constraints on Neutron star Matter with Existing and Upcoming Gravitational Wave and Pulsar Observations. *Phys. Rev. D* 101, 123007. doi:10.1103/PhysRevD.101.123007
- Lattimer, J. M., and Prakash, M. (2004). The Physics of Neutron Stars. *Science* 304, 536–542. doi:10.1126/science.1090720
- Lattimer, J. M. (2012). The Nuclear Equation of State and Neutron star Masses. *Annu. Rev. Nucl. Part. Sci.* 62, 485–515. doi:10.1146/annurev-nucl-102711-095018
- Lattimer, J. M. (2015). Introduction to Neutron Stars. *AIP Conf. Proc.* 1645, 61–78. doi:10.1063/1.4909560
- Le Fèvre, A., Leifels, Y., Reisdorf, W., Aichelin, J., and Hartnack, C. (2016). Constraining the Nuclear Matter Equation of State Around Twice Saturation Density. *Nucl. Phys. A* 945, 112–133. doi:10.1016/j.nuclphysa.2015.09.015
- Lim, Y., and Holt, J. W. (2018). Neutron star Tidal Deformabilities Constrained by Nuclear Theory and experiment. *Phys. Rev. Lett.* 121, 062701. doi:10.1103/PhysRevLett.121.062701
- Lindblom, L. (2018). Causal Representations of Neutron-star Equations of State. *Phys. Rev. D* 97, 123019. doi:10.1103/physrevd.97.123019
- Mareš, J., Friedman, E., Gal, A., and Jennings, B. (1995). Constraints on σ -nucleus Dynamics from Dirac Phenomenology of σ^- Atoms. *Nucl. Phys. A* 594, 311–324. doi:10.1016/0375-9474(95)00358-8
- Millener, D. J., Dover, C. B., and Gal, A. (1988). Λ -Nucleus Single-Particle Potentials. *Phys. Rev. C* 38, 2700–2708. doi:10.1103/PhysRevC.38.2700
- Miller, M. C., Lamb, F. K., Dittmann, A. J., Bogdanov, S., Arzoumanian, Z., Gendreau, K. C., et al. (2019). PSR J0030+0451 Mass and Radius from Nicer Data and Implications for the Properties of Neutron star Matter. *Astrophys. J.* 887, L24. doi:10.3847/2041-8213/ab50c5
- Miller, M. C., Chirenti, C., and Lamb, F. K. (2019). Constraining the Equation of State of High-Density Cold Matter Using Nuclear and Astronomical Measurements. *Astrophys. J.* 888, 12. doi:10.3847/1538-4357/ab4ef9
- Miller, M. C., Lamb, F. K., Dittmann, A. J., Bogdanov, S., Arzoumanian, Z., Gendreau, K. C., et al. (2021). The Radius of PSR J0740+6620 from Nicer and Xmm-newton Data. *Astrophys. J. Lett.* 918, L28. doi:10.3847/2041-8213/ac089b

- Most, E. R., Weih, L. R., Rezzolla, L., and Schaffner-Bielich, J. (2018). New Constraints on Radii and Tidal Deformabilities of Neutron Stars from Gw170817. *Phys. Rev. Lett.* 120, 261103. doi:10.1103/PhysRevLett.120.261103
- O'Boyle, M. F., Markakis, C., Stergioulas, N., and Read, J. S. (2020). Parametrized Equation of State for Neutron star Matter with Continuous Sound Speed. *Phys. Rev. D* 102, 083027. doi:10.1103/PhysRevD.102.083027
- Oertel, M., Hempel, M., Klähn, T., and Typel, S. (2017). Equations of State for Supernovae and Compact Stars. *Rev. Mod. Phys.* 89, 015007. doi:10.1103/RevModPhys.89.015007
- Özel, F., Baym, G., and Güver, T. (2010). Astrophysical Measurement of the Equation of State of Neutron star Matter. *Phys. Rev. D* 82, 101301. doi:10.1103/PhysRevD.82.101301
- Pang, P. T. H., Tews, I., Coughlin, M. W., Bulla, M., Van Den Broeck, C., and Dietrich, T. (2021). Nuclear Physics Multimessenger Astrophysics Constraints on the Neutron Star Equation of State: Adding NICER's PSR J0740+6620 Measurement. *Astro. Phys. J.* 922, 14. doi:10.3847/1538-4357/ac19ab
- Pradhan, B. K., and Chatterjee, D. (2021). Effect of Hyperons on *F*-Mode Oscillations in Neutron Stars. *Phys. Rev. C* 103, 035810. doi:10.1103/PhysRevC.103.035810
- Read, J. S., Lackey, B. D., Owen, B. J., and Friedman, J. L. (2009). Constraints on a Phenomenologically Parametrized Neutron-star Equation of State. *Phys. Rev. D* 79, 124032. doi:10.1103/physrevd.79.124032
- Riley, T. E., Watts, A. L., Bogdanov, S., Ray, P. S., Ludlam, R. M., Guillot, S., et al. (2019). A Nicer View of Psr J0030+0451: Millisecond Pulsar Parameter Estimation. *Astrophys. J.* 887, L21. doi:10.3847/2041-8213/ab481c
- Riley, T. E., Watts, A. L., Ray, P. S., Bogdanov, S., Guillot, S., Morsink, S. M., et al. (2021). A Nicer View of the Massive Pulsar Psr J0740+6620 Informed by Radio Timing and Xmm-newton Spectroscopy. *Astrophys. J. Lett.* 918, L27. doi:10.3847/2041-8213/ac0a81
- Rusotto, P., Gannon, S., Kupny, S., Lasko, P., Acosta, L., Adamczyk, M., et al. (2016). Results of the Asy-Eos experiment at Gsi: The Symmetry Energy at Suprasaturation Density. *Phys. Rev. C* 94. doi:10.1103/physrevc.94.034608
- Schaffner, J., Greiner, C., and Stöcker, H. (1992). Metastable Exotic Multihypernuclear Objects. *Phys. Rev. C* 46, 322–329. doi:10.1103/PhysRevC.46.322
- Schaffner, J., Dover, C. B., Gal, A., Greiner, C., and Stöcker, H. (1993). Strange Hadronic Matter. *Phys. Rev. Lett.* 71, 1328–1331. doi:10.1103/PhysRevLett.71.1328
- Schaffner-Bielich, J., and Gal, A. (2000). Properties of Strange Hadronic Matter in Bulk and in Finite Systems. *Phys. Rev. C* 62, 034311. doi:10.1103/PhysRevC.62.034311
- Schaffner-Bielich, J. (2020). *Compact Star Physics*. Cambridge, United Kingdom: Cambridge University Press. doi:10.1017/9781316848357
- Serot, B. D., and Walecka, J. D. (1992). Relativistic Nuclear many Body Theory. *Rec. Prog. Many Body Theor.* 3, 49–92. doi:10.1007/978-1-4615-3466-2_5
- Serot, B. D., and Walecka, J. D. (1997). Recent Progress in Quantum Hadrodynamics. *Int. J. Mod. Phys. E* 06, 515–631. doi:10.1142/s0218301397000299
- Steiner, A. W., Lattimer, J. M., and Brown, E. F. (2013). The Neutron star Mass-Radius Relation and the Equation of State of Dense Matter. *Astrophys. J.* 765, L5. doi:10.1088/2041-8205/765/1/L5
- Stone, J., and Reinhard, P. G. (2007). The Skyrme Interaction in Finite Nuclei and Nuclear Matter. *Prog. Part. Nucl. Phys.* 58, 587–657. doi:10.1016/j.pnpnp.2006.07.001
- Tews, I., Margueron, J., and Reddy, S. (2018). Critical Examination of Constraints on the Equation of State of Dense Matter Obtained from Gw170817. *Phys. Rev. C* 98, 045804. doi:10.1103/PhysRevC.98.045804
- Tews, I., Margueron, J., and Reddy, S. (2019). Constraining the Properties of Dense Matter and Neutron Stars by Combining Nuclear Physics and Gravitational Waves from Gw170817. *AIP Conf. Proc.* 2127, 020009. doi:10.1063/1.5117799
- Tews, I., Margueron, J., and Reddy, S. (2019). Confronting Gravitational-Wave Observations with Modern Nuclear Physics Constraints. *Eur. Phys. J. A* 55, 97. doi:10.1140/epja/i2019-12774-6
- Thorsett, S. E., and Chakrabarty, D. (1999). Neutron star Mass Measurements. I. Radio Pulsars. *Astrophys. J.* 512, 288–299. doi:10.1086/306742
- Tong, H., Zhao, P., and Meng, J. (2020). Symmetry Energy at Supra-saturation Densities via the Gravitational Waves from Gw170817. *Phys. Rev. C* 101, 035802. doi:10.1103/PhysRevC.101.035802
- Traversi, S., Char, P., and Pagliara, G. (2020). Bayesian Inference of Dense Matter Equation of State within Relativistic Mean Field Models Using Astrophysical Measurements. *Astrophys. J.* 897, 165. doi:10.3847/1538-4357/ab99c1
- Tsang, C. Y., Tsang, M. B., Danielewicz, P., Lynch, W. G., and Fattoyev, F. J. (2018). Constraining Neutron-star Equation of State Using Heavy-Ion Collisions. arXiv e-prints. arXiv:1807.06571.
- Vautherin, D., and Brink, D. M. (1972). Hartree-fock Calculations with Skyrme's Interaction. I. Spherical Nuclei. *Phys. Rev. C* 5, 626–647. doi:10.1103/PhysRevC.5.626
- Wei, J. B., Lu, J. J., Burgio, G. F., Li, Z. H., and Schulze, H. J. (2020). Are Nuclear Matter Properties Correlated to Neutron star Observables? *Eur. Phys. J. A.* 56, 63. doi:10.1140/epja/s10050-020-00058-3
- Weissenborn, S., Chatterjee, D., and Schaffner-Bielich, J. (2012). Hyperons and Massive Neutron Stars: The Role of Hyperon Potentials. *Nucl. Phys. A* 881, 62–77. doi:10.1016/j.nuclphysa.2012.02.012
- Xie, W. J., and Li, B. A. (2019). Bayesian Inference of High-Density Nuclear Symmetry Energy from Radii of Canonical Neutron Stars. *Astrophys. J.* 883, 174. doi:10.3847/1538-4357/ab3f37
- Yagi, K., and Yunes, N. (2013). I-love-q Relations in Neutron Stars and Their Applications to Astrophysics, Gravitational Waves, and Fundamental Physics. *Phys. Rev. D* 88, 023009. doi:10.1103/PhysRevD.88.023009
- Zhang, N. B., and Li, B. A. (2019). Implications of the Mass $M = 2.17 + 0.11 - 0.10 M_{\odot}$ of Psr J0740+6620 on the Equation of State of Super-dense Neutron-Rich Nuclear Matter. *Astrophys. J.* 879, 99. doi:10.3847/1538-4357/ab24cb
- Zhu, Z. Y., Zhou, E. P., and Li, A. (2018). Neutron star Equation of State from the Quark Level in Light of Gw170817. *Astrophys. J.* 862, 98. doi:10.3847/1538-4357/aacc28
- Zimmerman, J., Carson, Z., Schumacher, K., Steiner, A. W., and Yagi, K. (2020). Measuring Nuclear Matter Parameters with NICER and LIGO/Virgo. arXiv e-prints. arXiv:2002.03210.

Conflict of Interest: The authors declare that the research was conducted in the absence of any commercial or financial relationships that could be construed as a potential conflict of interest.

Publisher's Note: All claims expressed in this article are solely those of the authors and do not necessarily represent those of their affiliated organizations or those of the publisher, the editors, and the reviewers. Any product that may be evaluated in this article, or claim that may be made by its manufacturer, is not guaranteed or endorsed by the publisher.

Copyright © 2022 Ghosh, Pradhan, Chatterjee and Schaffner-Bielich. This is an open-access article distributed under the terms of the Creative Commons Attribution License (CC BY). The use, distribution or reproduction in other forums is permitted, provided the original author(s) and the copyright owner(s) are credited and that the original publication in this journal is cited, in accordance with accepted academic practice. No use, distribution or reproduction is permitted which does not comply with these terms.